Geophysical Research Letters

RESEARCH LETTER
10.1029/2020GL090190

# Rapid Landau Heating of Martian Topside Ionospheric Electrons by Large-Amplitude Magnetosonic Waves

**Zhenpeng Su[1,2], Nigang Liu[1,2,3], Zhonglei Gao[4], Bin Wang[5], Huinan Zheng[1,2], Yuming Wang[1,2], and Shui Wang[1,2]**

[1]CAS Key Laboratory of Geospace Environment, Department of Geophysics and Planetary Sciences, University of Science and Technology of China, Hefei, China, [2]CAS Center for Excellence in Comparative Planetology, University of Science and Technology of China, Hefei, China, [3]Anhui Mengcheng Geophysics National Observation and Research Station, University of Science and Technology of China, Mengcheng, China, [4]School of Physics and Electronic Sciences, Changsha University of Science and Technology, Changsha, China, [5]Beijing Institute of Tracing and Telecommunications Technology, Beijing, China

**Key Points:**

- Magnetosonic waves are difficult to cyclotron-resonate with Martian ionospheric oxygen atomic and molecular ions below the escape energies
- Strong magnetosonic waves can Landau-heat Martian topside ionospheric electrons to 2 times the normal temperature over tens of minutes
- Electron Landau heating by magnetosonic waves may facilitate the Martian ionospheric erosion by enhancing the ambipolar electric field

**Correspondence to:**
Z. Su,
szpe@mail.ustc.edu.cn

**Citation:**
Su, Z., Liu, N., Gao, Z., Wang, B., Zheng, H., Wang, Y., & Wang, S. (2020). Rapid Landau heating of Martian topside ionospheric electrons by large-amplitude magnetosonic waves. *Geophysical Research Letters*, *47*, e2020GL090190. https://doi.org/10.1029/2020GL090190

Received 4 AUG 2020
Accepted 3 OCT 2020
Accepted article online 9 OCT 2020

**Abstract** Atmospheric escape is a fundamental process in the long-term habitability evolution of terrestrial planets. Recent observations on Mars have found the concurrence of the severe ionospheric erosion and the large-amplitude, quasi-perpendicular magnetosonic waves. However, whether and then how these magnetosonic waves had contributed to the ionospheric erosion remains unclear. Here we propose a new candidate mechanism, electron Landau heating by magnetosonic waves, for the Martian ionospheric erosion. In contrast to the cyclotron resonance with oxygen atomic and molecular ions above the escape energies, the magnetosonic waves Landau-resonate with the thermal electrons at energy channels of the order of 0.01–0.1 eV. Through the Landau resonance over tens of minutes, the large-amplitude (12 nT) magnetosonic waves can heat the topside ionospheric electrons to ~2 times the normal temperature. The topside ionospheric electron heating could result in the enhancement of the ambipolar electric potential and eventually facilitate the escape of ionospheric plasma.

**Plain Language Summary** An atmosphere of sufficient density is a fundamental condition for a habitable terrestrial planet. Mars as a terrestrial planet in the habitable zone of our solar system lost much of its atmosphere over billions of years and has thus become a unique testing ground to understand the planetary atmospheric loss processes. Recent observations on Mars have shown that the severe erosion of the ionosphere, an ionized part of the upper atmosphere, was accompanied by the large-amplitude, quasi-perpendicular magnetosonic waves. However, whether and then how these magnetosonic waves had contributed to the ionospheric erosion remains unclear. On the basis of space observations and numerical calculations, we propose a new physical mechanism, electron Landau heating by magnetosonic waves, for the Martian ionospheric erosion. The large-amplitude magnetosonic waves can heat the topside ionospheric electrons to ~2 times the normal temperature over tens of minutes, enhance the ambipolar electric potential, and eventually facilitate the escape of ionospheric plasma. The electron Landau heating process may also contribute to the ionospheric erosion of other terrestrial planets within and beyond our solar system.

## 1. Introduction

Mars is a terrestrial planet located in the habitable zone of our solar system. Compared with Earth, Mars has approximately 40% of the gravity but less than 1% of the atmospheric density at its surface. Mars has thus become a unique testing ground to understand the atmospheric loss processes of terrestrial planets. In the past several decades, two classes of loss processes driven by solar wind and radiation have been proposed (Jakosky et al., 2018; Shizgal & Arkos, 1996): thermal processes including evaporative escape (Jeans, 1925) and hydrodynamic escape (Pepin, 1991); nonthermal processes including photochemical escape (Cui et al., 2019; Johnson et al., 2008; McElroy, 1972), ion sputtering (Luhmann et al., 1992), and ion heating or acceleration (Brain et al., 2015; Lundin et al., 2004; Wei et al., 2012).

In recent years, plasma waves have been envisioned to heat or accelerate the Martian ionospheric plasma (Ergun et al., 2006; Espley et al., 2004; Fowler, Andersson, Peterson, et al., 2018; Lundin et al., 2011),

©2020. American Geophysical Union. All Rights Reserved.

by analogy with Earth (André & Yau, 1997; Yau & André, 1997). One of the frequently observed waves in the Martian ionosphere is the magnetosonic wave (Bertucci et al., 2004; Collinson et al., 2018; Fowler, Andersson, Ergun, et al., 2018; Halekas et al., 2011). These magnetosonic waves are probably produced by the solar wind near the parallel foreshock and propagate through the magnetosheath into the ionosphere (Brain et al., 2002; Collinson et al., 2018; Luhmann et al., 1983). They usually have the large normal angles of >50° and the magnetic amplitudes of 2–15 nT (Collinson et al., 2018; Fowler, Andersson, Ergun, et al., 2018). However, how the magnetosonic waves contribute to the Martian atmospheric loss remains under debate. Fowler, Andersson, Ergun, et al. (2018) suggested that the cyclotron resonant interactions between magnetosonic waves and heavy ions were responsible for the observed severe ionospheric erosion. On the contrary, Collinson et al. (2018) hypothesized the energy transfer from the magnetosonic waves to the ionospheric plasma through some adiabatic compression processes rather than the wave-particle resonances. More recently, Fowler et al. (2020) proposed that a combination of the adiabatic magnetic pumping by the large-amplitude magnetosonic waves and the pitch angle scattering by the induced whistler waves could heat the ionospheric suprathermal electrons.

In this letter, on the basis of observations from Mars Atmosphere and Volatile EvolutioN (MAVEN) mission (Jakosky, Lin, et al., 2015) and calculations of Waves in Homogeneous, Anisotropic, Multicomponent Plasmas (WHAMP) code (Rönnmark, 1982), we show that the large-amplitude magnetosonic waves are able to rapidly heat the Martian ionospheric electrons through Landau resonances. The heating of topside ionospheric electrons may favor the buildup of an ambipolar electric field and eventually assist the escape of heavy ions (Collinson et al., 2019; Moore et al., 1997).

## 2. MAVEN Observations

On 21 September 2014, the MAVEN mission entered the Mars orbit with apoapsis altitude of ~6,200 km and periapsis altitude of ~150 km (Jakosky, Grebowsky, et al., 2015; Jakosky, Lin, et al., 2015). In this letter, we analyze the particle and magnetic field data from MAVEN in the Martian ionosphere. The electron density $N_e$ and temperature $T_e$ were measured by the Langmuir Probe and Waves instrument (Andersson et al., 2015; Ergun et al., 2015), the density of oxygen atomic $N_{O^+}$ and molecular ions $N_{O_2^+}$ and hydrogen ions $N_{H^+}$ were measured by the SupraThermal And Thermal Ion Composition instrument (McFadden et al., 2015), and the magnetic field **B** was measured by the Magnetometer instrument (Connerney, Espley, DiBraccio, et al., 2015; Connerney, Espley, Lawton, et al., 2015).

In Figure 1, we revisit the 1 April 2015 event reported early by Fowler, Andersson, Ergun, et al. (2018). In the plotted time range from 05:50 UT to 06:00 UT, MAVEN was sampling the dayside (with the solar zenith angle $\Theta_Z = 15$–$30°$) ionosphere (with the altitude $H = 592$–$196$ km). Only the $O^+$ and $O_2^+$ density data were available, and the $H^+$ density likely became too low to be measured (Figure 1a). Note that $O^+$ and $O_2^+$ are typically the major ion species in the Martian ionosphere (e.g., Benna et al., 2015). The summation of these ion densities deviated obviously from the electron density (Figure 1b), probably because of the instrument calibration issues. Under the action of solar radiation, the electron density profile typically exhibits two peaks: the main layer M2 of ~130 km altitude and the secondary layer M1 of ~100 km altitude, which can be well characterized by the Chapman photo-equilibrium model (Gurnett et al., 2008; Withers, 2009). Because of the dominance of transport processes roughly above 200 km, the electron density decreases exponentially with increasing altitude (Fox, 1997; Withers, 2009). Ergun et al. (2015) had adopted a Chapman model to fit the electron density profile during the MAVEN deep dip campaign from 15 to 22 April 2015

$$N_e = N_{e1} + N_{e2}, \tag{1}$$

$$N_{ei} = N_i \exp\left[\frac{1}{2}\left(1 - \frac{H - H_i}{H_{ci}} - \exp\left(-\frac{H - H_i}{H_{ci}}\right)\right)\right], \tag{2}$$

with the subscripts "1" and "2" for M1 and M2 layers and the specific parameters $N_1 = 5 \times 10^4$ cm$^{-3}$, $H_1 = 106$ km, $H_{c1} = 7.7$ km, $N_2 = 2.6 \times 10^5$ cm$^{-3}$, $H_2 = 124$ km, and $H_{c2} = 12.6$ km. Under the quiet condition on 31 March 2015, the electron density profile deviated significantly from the Chapman model above 200 km, consistent with the finding of Ergun et al. (2015). Compared to the ionospheric passes in the previous day, this inbound pass on 1 April 2015 had several orders of magnitude lower electron densities above the altitude $H$ of 260 km. The remnant electrons below 380 km tended to obey the specific Chapman model given by

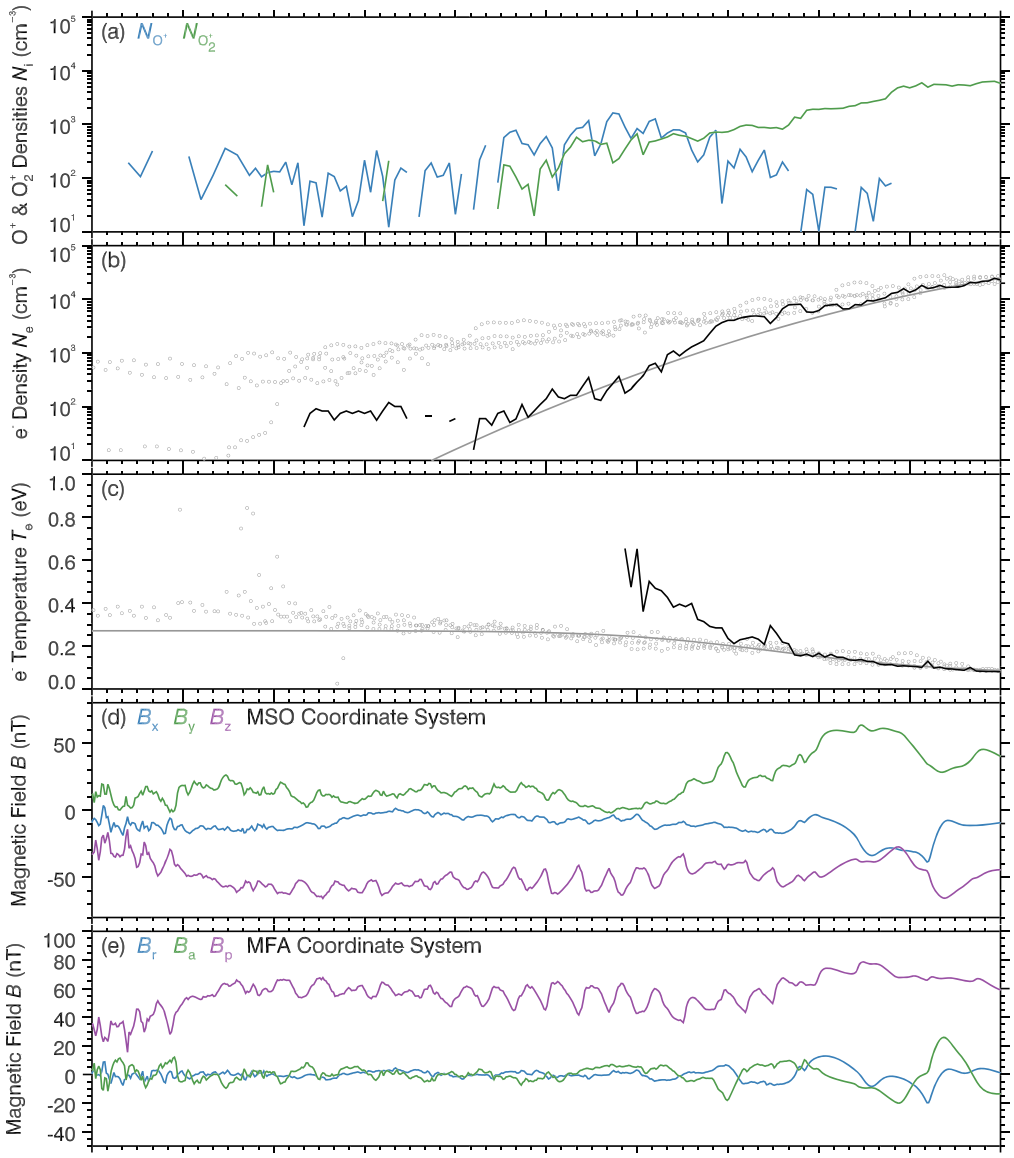


| UT | 05:50 | 05:51 | 05:52 | 05:53 | 05:54 | 05:55 | 05:56 | 05:57 | 05:58 | 05:59 | 06:00 |
|---|---|---|---|---|---|---|---|---|---|---|---|
| $X_{MSO}$ (km) | 3700.0 | 3700.0 | 3690.0 | 3661.3 | 3631.3 | 3590.0 | 3540.0 | 3471.3 | 3401.3 | 3311.3 | 3220.0 |
| $Y_{MSO}$ (km) | 88.5 | 243.2 | 396.8 | 549.8 | 700.8 | 849.8 | 996.8 | 1138.8 | 1278.8 | 1418.8 | 1548.8 |
| $Z_{MSO}$ (km) | -1461.9 | -1291.3 | -1111.3 | -930.5 | -745.6 | -559.5 | -370.6 | -181.6 | 8.2 | 198.4 | 387.4 |
| $H$ (km) | 591.5 | 533.8 | 479.2 | 428.3 | 381.3 | 338.5 | 300.1 | 266.5 | 237.8 | 214.4 | 196.4 |
| $\Theta_z$ (Deg) | 21.6 | 19.6 | 17.8 | 16.4 | 15.7 | 15.8 | 16.7 | 18.4 | 20.6 | 23.3 | 26.4 |

**Figure 1.** An overview of the Martian ionospheric environment from 05:50 UT to 06:00 UT on 1 April 2015: (a) oxygen atomic and molecular ion densities $N_{O^+}$ and $N_{O_2^+}$ (color-coded); (b) electron density $N_e$ (solid line), compared with the data from the previous day under the quiet condition (gray circles) and the Chapman model of Ergun et al. (2015) (gray line); (c) electron temperature $T_e$, compared with the data from the previous day under the quiet condition (gray circles) and the hyperbolic tangent model of Ergun et al. (2015) (gray line); (d) magnetic field components $(B_x, B_y, B_z)$ in the Mars Solar Orbital (MSO) coordinate system (color-coded); (e) magnetic field components $(B_r, B_a, B_p)$ in the Mean Field Aligned (MFA) coordinate system (color-coded). The MSO coordinate system is defined with the $x$ axis pointing from Mars to the Sun, the $y$ axis pointing antiparallel to Martian orbital velocity, and the $z$ axis completing the triad. The MFA coordinate system is defined with the $p$ axis parallel to the 90 s running average of the instantaneous magnetic field, the $a$ axis determined by the cross product of the parallel vector and the satellite position vector, and the $r$ axis completing the triad.

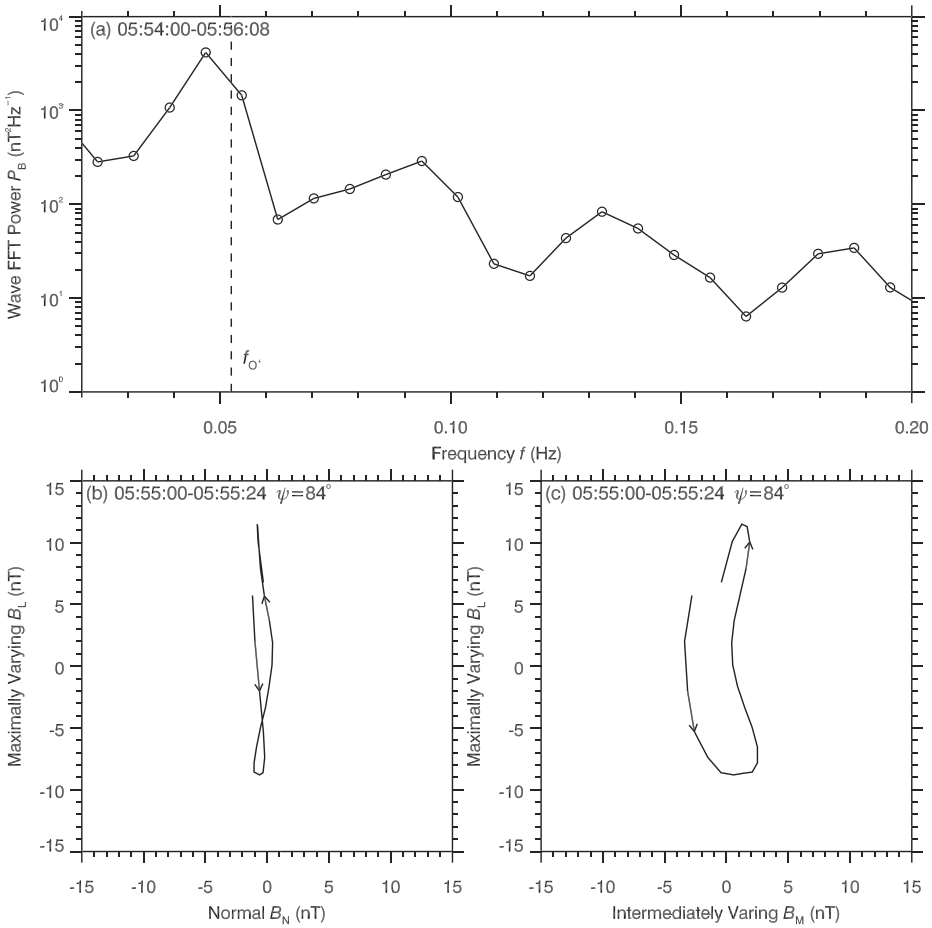


**Figure 2.** Magnetosonic wave properties: (a) wave power $P_B$ depending on frequency $f$ during 05:54:00–05:56:08 UT, with the vertical dashed line marking the oxygen atomic ion gyrofrequency $f_{O^+}$; (b, c) normal $B_N$, intermediately varying $B_M$, and maximally varying $B_L$ components of wave magnetic fields in the minimum variance coordinate system during 05:55:00–05:55:24 UT, with the wave normal angle determined as $\psi = 84°$.

Ergun et al. (2015). For the MAVEN deep dip campaign, Ergun et al. (2015) had introduced a hyperbolic tangent model of the electron temperature

$$T_e = \frac{T_{eU} + T_{eL}}{2} + \frac{T_{eU} - T_{eL}}{2} \tanh\left(\frac{H - H_0}{H_{c0}}\right) \quad (3)$$

with $T_{eU} = 0.271$ eV, $T_{eL} = 0.044$ eV, $H_0 = 241$ km, and $H_{c0} = 60$ km. In the quiet ionosphere on 31 March 2015, the electron temperature profile agreed well with the model prediction (Figure 1c). In contrast, the electron temperature of the eroded ionosphere on 1 April 2015 increased steeply with the altitude increasing. At $H = 300$ km, the electron temperature increased to 0.45–0.60 eV, more than 2 times the previous-day value. Above $H = 300$ km, the electron temperature had become too high to be measured (Fowler, Andersson, Ergun, et al., 2018). Corresponding to the ionospheric erosion, there were waves with the large-amplitude (up to 12 nT), sawtooth magnetic perturbations $\mathbf{B}_W$ primarily along the background magnetic field (Figures 1d and 1e).

In Figure 2, we determine the frequency, propagation, and polarization characteristics of waves for the subsequent calculations. We apply the fast Fourier transform to the largest perturbations during 05:54:00–05:56:08 UT and obtain the harmonically structured wave power with the fundamental frequency of 0.046 Hz $\approx 0.88 f_{O^+}$ ($f_{O^+}$ is the $O^+$ gyrofrequency). We perform the minimum variance analysis (Sonnerup & Cahill, 1967) to the magnetic perturbations, approximate the wave vector to be parallel to the minimum varying component, and then estimate the wave normal angle to be $\psi = 84°$. In the plane perpendicular to the normal component, we find the highly elliptically polarized perturbations. These observations indicate that the observed large-amplitude waves were the quasi-perpendicular, compressional magnetosonic waves.

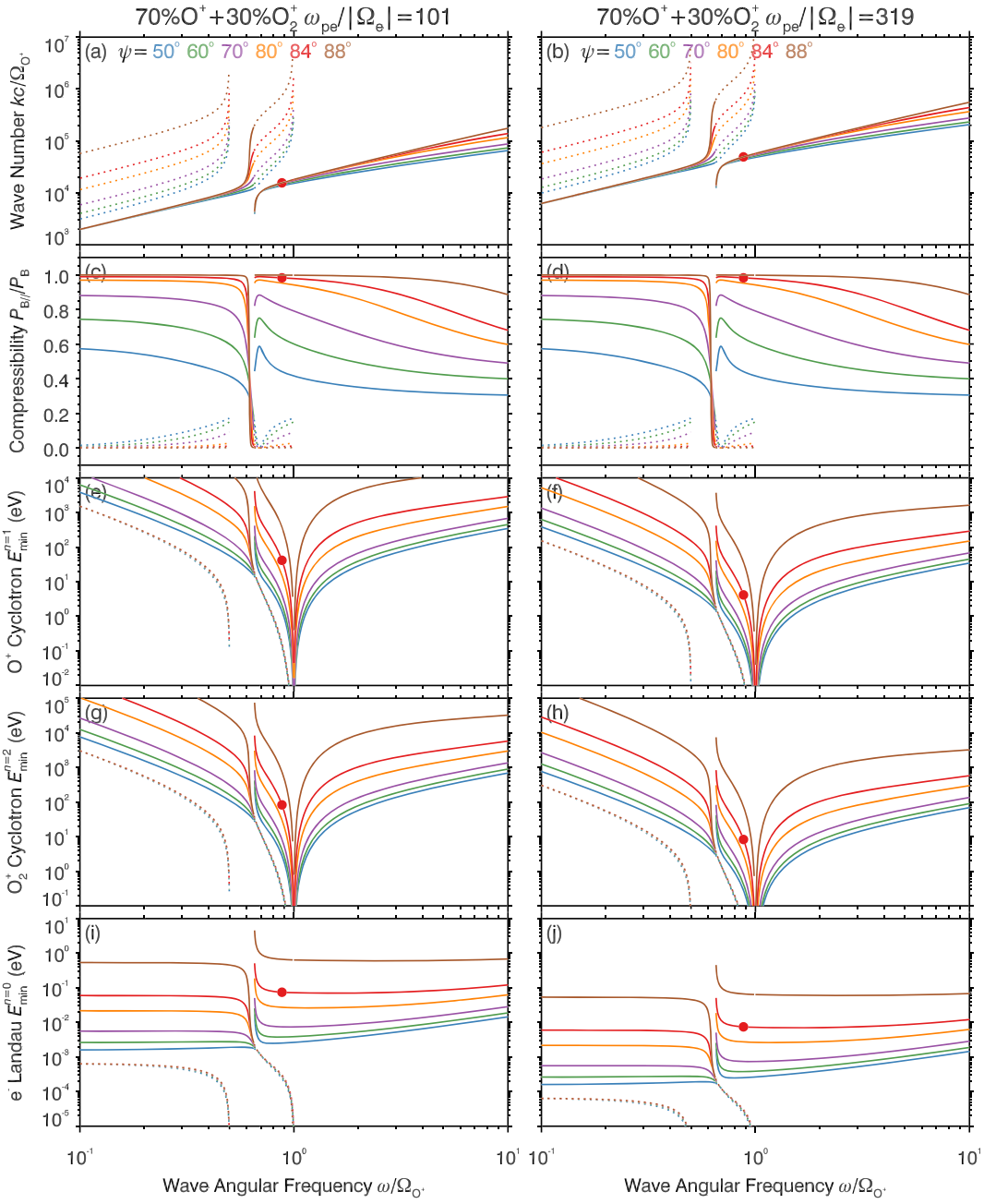


**Figure 3.** Properties of compressional (solid lines) and noncompressional (dashed lines) waves at different normal angles (color-coded) in the cold plasma with low (left) and high (right) densities: (a, b) dependence of wave number $kc/\Omega_{O^+}$ on wave angular frequency $\omega/\Omega_{O^+}$; (c, d) ratio between parallel and total wave power $P_{B//}/P_B$ depending on $\omega/\Omega_{O^+}$; (e, f, g, h) minimum cyclotron resonant energy of oxygen atomic and molecular ions $E_{min}$ depending on $\omega/\Omega_{O^+}$; (i, j) minimum Landau resonant energy of electrons $E_{min}$ depending on $\omega/\Omega_{O^+}$. The red dots mark the properties of observed magnetosonic waves during 05:55:00–05:55:24 UT on 1 April 2015.

## 3. Numerical Calculations

The MAVEN observations indicate the concurrence of the large-amplitude magnetosonic waves and the severe ionospheric erosion, but whether and how these magnetosonic waves had contributed to the ionospheric erosion remains unclear. Figure 3 shows a parametric analysis about the wave properties and the minimum resonant energies (Summers et al., 2007a, 2007b) in the framework of cold-plasma theory. According to observations at $H = 300$ km (Figure 1), the magnetic field strength $B$ is set to 55 nT, the ion

compositions are set to 70%$O^+$+30%$O_2^+$, and the electron density is set to 300 $cm^{-3}$ for the eroded ionosphere and 3,000 $cm^{-3}$ for the normal ionosphere. The corresponding ratio of the electron plasma frequency to the electron gyrofrequency $\omega_{pe}/|\Omega_e|$, a commonly used dimensionless parameter, has the values of 101 and 319 in the eroded and normal ionospheres. According to the compressibility defined as the ratio of parallel to total magnetic power $P_{B\|}/P_B$, the allowed plasma waves are classified into the compressional and noncompressional types. Specifically, when two wave modes arise in the frequency range of interest, the mode with a lower $P_{B\|}/P_B$ is defined as the noncompressional mode and the other mode is defined as the compressional mode; the identified compressional mode can extend along the dispersion curve over a broader frequency range where the noncompressional mode is forbidden. For the quasi-perpendicular waves (except near the cutoff frequency), $P_{B\|}/P_B$ is close to 1 at the compressional mode and falls to 0 at the noncompressional mode. As the normal angle decreases, $P_{B\|}/P_B$ decreases at the compressional mode but increases at the noncompressional mode. The linear resonant condition between waves and particles can be written as

$$\omega - k_{\|} v_{\|} = n\Omega_s, \tag{4}$$

with the wave angular frequency $\omega$, the parallel wave vector $k_{\|} = k\cos\psi$, the angular gyrofrequency of particles $\Omega_s = \frac{q_s B}{m_s}$, the parallel velocity of particles $v_{\|}$, and the resonance order $n$. From the resonant condition above, we can determine the parallel velocity of the particles falling into the $n$th order resonance

$$v_{\|} = \frac{\omega - n\Omega_s}{k_{\|}}. \tag{5}$$

Because of no constraint on the perpendicular velocity $v_{\perp}$ in the linear resonance theory, the energy of resonant particles reaches the minimum at $v_{\perp} = 0$ (Summers et al., 2007a, 2007b)

$$E_{\min} = \frac{1}{2} m_s v_{\|}^2 = \frac{1}{2} m_s \left( \frac{\omega - n\Omega_s}{k_{\|}} \right)^2. \tag{6}$$

Except near the cutoff frequency, the dispersion relation of the highly oblique, compressional waves can be approximately written as

$$\omega \approx k_{\perp} v_A, \tag{7}$$

with the perpendicular wave vector $k_{\perp} = k\sin\psi$ and the Alfvén velocity $v_A$. Substituting Equation 7 into Equation 6 yields

$$E_{\min} \approx \frac{1}{2} m_s \left[ \left( 1 - n\frac{\Omega_s}{\omega} \right) v_A \tan\psi \right]^2. \tag{8}$$

For the observed waves with the fundamental frequency $\omega \approx 0.88\Omega_{O^+}$ among all the resonance orders, $E_{\min}$ reaches the valley at $n = 1, 2$, and 0 for $O^+$, $O_2^+$, and $e^-$, respectively. With the dispersion relation in Figures 3a and 3b, we calculate the corresponding minimum resonant energies (Figures 3e–3j) from Equation 6. The minimum resonant energies of $O^+$ and $O_2^+$ are 4 and 8 eV in the normal ionosphere and increase to 30 and 80 eV in the eroded ionosphere, which are 2–20 times larger than the corresponding escape energies. The expected cyclotron resonant interactions below the escape energies of $O^+$ and $O_2^+$ could occur only when the wave frequencies are sufficiently close to the gyrofrequency harmonics or the wave normal angles are sufficiently low. In the normal topside ionosphere, the ion temperature is quite close to the electron temperature of ~0.25 eV (Hanson et al., 1977). The magnetosonic waves seem to be difficult to directly accelerate the ions from the thermal energy to the escape energy through the cyclotron resonance. In contrast, for the Landau resonance with $e^-$, the minimum resonant energies of the compressional waves are largely independent of the wave frequency and have values comparable to the electron temperature in both the normal and eroded ionospheres. As a result, the Martian ionospheric thermal electrons should substantially Landau-damp the magnetosonic waves.

Although the magnetosonic waves had the waveforms deviating obviously from the sinusoidal pattern (Figure 1d), their Landau damping rates may still be reasonably estimated by the linear theory (Matsumoto & Nagai, 1981). Similar to Figure 3, Figure 4 shows a parametric analysis by WHAMP code (Rönnmark, 1982)

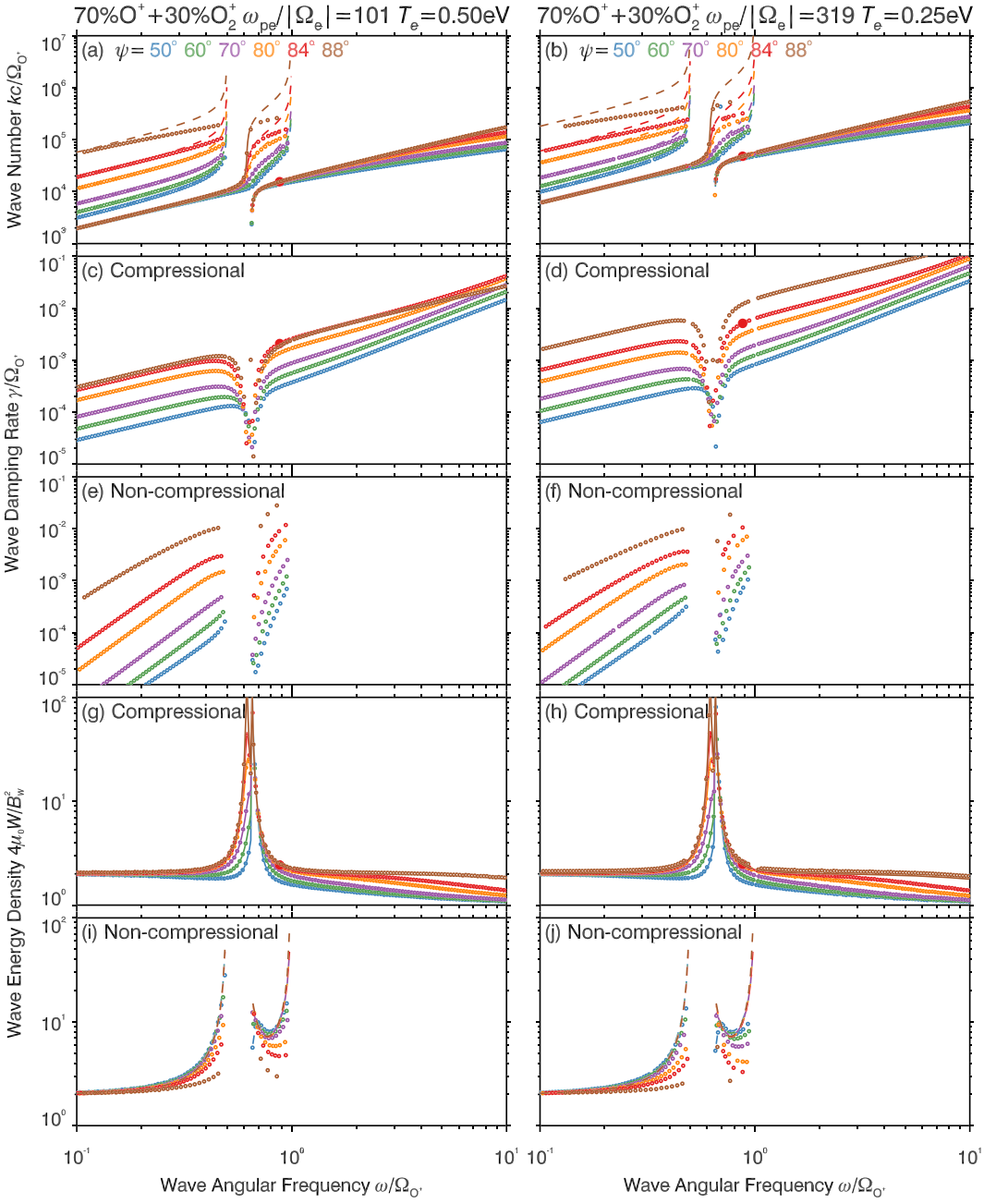


**Figure 4.** Properties of waves at different normal angles (color-coded) in the hot plasma with low (left) and high (right) densities: (a, b) dependence of wave number $kc/\Omega_{O^+}$ on wave angular frequency $\omega/\Omega_{O^+}$ (circles), compared with the cold-plasma approximation (solid lines for compressional waves and dashed lines for noncompressional waves); (c, d) compressional and (e, f) noncompressional wave damping rate $\gamma/\Omega_{O^+}$ (circles) depending on $\omega/\Omega_{O^+}$; (g, h) compressional and (i, j) noncompressional wave energy density $4\mu_0 W/B_W^2$ (circles), compared with the cold-plasma approximation (solid and dashed lines). The red dots mark the properties of observed magnetosonic waves during 05:55:00–05:55:24 UT on 1 April 2015.

of the wave dispersion relations, the wave damping rates, and the wave energy densities in the hot plasma. The WHAMP code includes several populations of particles obeying the subtracted Maxwellian distribution (Ashour-Abdalla & Kennel, 1978) and solves the linear analytic dispersion equation of waves in homogeneous magnetized hot plasmas. Keeping the wave vector **k** real, the WHAMP can find the complex wave frequency $\omega - i\gamma$, where $\gamma$ is the wave temporal damping rate. The total wave energy density $W$ contains

both the electromagnetic and acoustic contributions (Stix, 1992)

$$W = \frac{\epsilon_0}{4}\mathbf{E}_{\mathrm{W}}^{*} \cdot \frac{\partial}{\partial \omega}\left(\omega \epsilon_{\mathrm{h}}\right) \cdot \mathbf{E}_{\mathrm{W}} + \frac{|\mathbf{B}_{\mathrm{W}}|^2}{4\mu_0}, \tag{9}$$

$$\epsilon_{\mathrm{h}} = \frac{1}{2}\left(\epsilon + \epsilon^{\dagger}\right), \tag{10}$$

with the electromagnetic vectors of waves $\mathbf{E}_{\mathrm{W}}$ and $\mathbf{B}_{\mathrm{W}}$, the plasma dielectric tensor $\epsilon$, the superscripts representing the complex * and Hermitian † conjugates, and the vacuum permittivity $\epsilon_0$ and permeability $\mu_0$. For simplicity, we assume both electron and ion distributions are isotropic. According to the MAVEN observations (Figure 1), we set the electron temperature $T_{\mathrm{e}} = 0.50$ and 0.25 eV and in the eroded and normal ionospheres. To exclude the hot-ion effect, we have artificially set all the ion temperatures to $T_{\mathrm{O}^+} = T_{\mathrm{O}_2^+} = 10^{-6}$ eV. Contrary to the noncompressional waves, the compressional waves have the dispersion relations changing little from the cold to hot plasma. Because the wave resonant energies are comparable to or much less than the electron temperature, both the compressional and noncompressional waves experience the strong Landau damping. The damping rate tends to increase with the normal angle increasing. For the observed waves with the fundamental frequency $\omega \approx 0.88\Omega_{\mathrm{O}^+}$ and the normal angle $\psi = 84°$, the total wave energy densities $W$ are always about 2 times the wave magnetic energy density $\frac{|\mathbf{B}_{\mathrm{W}}|^2}{4\mu_0}$, and the dimensionless Landau damping rates $\gamma/\Omega_{\mathrm{O}^+}$ reach $2\times10^{-3}$ and $5\times10^{-3}$ in the eroded and normal ionospheres. In the solar wind (Matsumoto & Nagai, 1981), Earth's magnetosphere (Dai et al., 2019; Horne et al., 2000, 2007) and laboratory plasmas (Porkolab, 1994), the magnetosonic waves have been suggested to heat electrons through the Landau resonance. By analogy, we can expect the electron Landau heating by magnetosonic waves in the Martian ionosphere.

## 4. Discussion

In the linear theory (Shklyar, 2017; Stix, 1992), the rate of change of kinetic energy density of the particles $P_{\mathrm{WP}}$ driven by the wave resonant interactions may be approximately written as

$$P_{\mathrm{WP}} = 2\gamma W. \tag{11}$$

With $\Omega_{\mathrm{O}^+} = 0.32$ rad·s$^{-1}$ and $B_{\mathrm{W}} = 12$ nT observed on 1 April 2015, we dimensionalize the damping rate $\gamma$ and energy density $W$ of Figures 4c, 4d, 4g, and 4h, and from Equation 11, obtain the change rate of electron kinetic energy density $P_{\mathrm{WP}} = 0.45$ and 1.14 eV·cm$^{-3}$·s$^{-1}$ in the eroded and normal ionospheres. The time required for the large-amplitude magnetosonic waves to cause a temperature enhancement $\Delta T_{\mathrm{e}}$ of the ionospheric electrons with a constant-density $N_{\mathrm{e}}$ can be estimated as

$$\Delta t = \frac{\frac{3}{2}N_{\mathrm{e}}\Delta T_{\mathrm{e}}}{P_{\mathrm{WP}}}. \tag{12}$$

Taking $\Delta T_{\mathrm{e}} = 0.25$ eV (Figure 1), $\Delta t = 16$ min for the normal density $N_{\mathrm{e}} = 3\times10^3$ cm$^{-3}$ and $\Delta t = 4.1$ min for the eroded density $N_{\mathrm{e}} = 3\times10^2$ cm$^{-3}$. Because of the potential cross-species or cross-region energy transfer, the required time in reality would be higher to some extent than the present estimation. In all the calculations above, we have ignored the possible change of ion compositions during the ionospheric erosion. The decrease of mass density would enlarge the Alfven velocity $v_{\mathrm{A}}$, increase the minimum resonant energy $E_{\mathrm{min}}$, lower the wave damping rate $\gamma$, and prolong more or less the required heating time $\Delta t$. Nevertheless, these calculations support the possibility that the Landau heating of the large-amplitude magnetosonic waves on a timescale of tens of minutes could explain the observed topside ionospheric electron temperature variation (Figure 1c).

The parallel ambipolar electric field along a draped field line can be expressed as (e.g., Collinson et al., 2019; Gombosi & Nagy, 1989; Liemohn et al., 1997; Varney et al., 2014)

$$E_{\parallel} = -\frac{1}{eN_{\mathrm{e}}}\frac{\partial p_{\mathrm{e}}}{\partial s} \tag{13}$$

with the electron pressure $p_{\mathrm{e}} = N_{\mathrm{e}}T_{\mathrm{e}}$ and the field line length $s$. For the normal Martian ionosphere with the topside electron temperature ~0.25 eV, the electric potential drop $\Phi = \int E_{\parallel} ds$ is about 0.7 V (Collinson

et al., 2019; Ergun et al., 2015). When the topside electron temperature increases to ~0.5 eV or more (Figure 1c), a first-order approximation of the corresponding potential drop is 1.4 V or more. Since the escape energy for oxygen from Mars is 1.91 eV, the electron Landau heating by the large-amplitude magnetosonic waves could substantially promote the erosion of the Martian ionosphere.

## 5. Summary

Fowler, Andersson, Ergun, et al. (2018) have reported the concurrence of the large-amplitude magnetosonic waves and the severe erosion of the Martian topside ionosphere on 1 April 2015. Our present study attempts to examine whether and then how these magnetosonic waves had contributed to the ionospheric erosion. At the altitude of ~300 km on the dayside, the magnetosonic waves exhibited a sawtooth waveform with the peak amplitude of ~12 nT and the primary frequency of 0.88 $f_{O^+}$ and propagated in the quasi-perpendicular normal angle of 84° with respect to the draped magnetic field lines. Because of the unignorable frequency difference from the ion gyrofrequency harmonics and the large normal angles, these waves are found to be difficult to cyclotron-resonate with $O^+$ and $O_2^+$ below the escape energies. In contrast, these waves could easily fall into Landau resonance with the thermal electrons at energy channels of the order of 0.01–0.1 eV. The Landau damping rates of magnetosonic waves reach $2 \times 10^{-3}\Omega_{O^+}$ and $5 \times 10^{-3}\Omega_{O^+}$ in the eroded (low-density) and normal (high-density) ionospheres. On a time scale of tens of minutes, the large-amplitude magnetosonic waves can provide sufficient energy for the observed ~2-time enhancement in the ionospheric electron temperature. The topside ionospheric electron heating may increase the ambipolar electric potential and then substantially facilitate the ionospheric erosion. In spite of the limitation to parametric and idealized calculations, our study has provided a new candidate mechanism, Landau heating of electrons by magnetosonic waves, for the Martian ionospheric erosion. Future theoretical, observational, and modeling works are required to quantitatively evaluate the contributions of these physical mechanisms proposed here and previously (e.g., Collinson et al., 2018; Fowler, Andersson, Ergun, et al., 2018; Fowler et al., 2020) to the evolution of the Martian ionosphere.

## Data Availability Statement

MAVEN data were obtained from the website https://lasp.colorado.edu/maven/sdc/public/data/sci/, and WHAMP code was obtained online (from the website https://github.com/irfu/whamp).

**Acknowledgments**
We acknowledge B. M. Jakosky, L. Andersson, J. McFadden, and J. E. P. Connerney for providing the MAVEN data and acknowledge K. Rönnmark for the use of WHAMP code. This work was supported by the Strategic Priority Research Program of Chinese Academy of Sciences grant XDB 41000000, the National Natural Science Foundation of China grants 41774170 and 41631071, the Chinese Academy of Sciences grant KZCX2-EW-QN510 and KZZD-EW-01-4, the CAS Key Research Program of Frontier Sciences grant QYZDB-SSW-DQC015, the National Key Basic Research Special Foundation of China Grant No. 2011CB811403, the National Postdoctoral Program for Innovative Talents Grant BX20190310, and the China Postdoctoral Science Foundation Grant No. 2019M662171.

## References

Andersson, L., Ergun, R. E., Delory, G. T., Eriksson, A., Westfall, J., Reed, H., & Meyers, D. (2015). The Langmuir Probe and Waves (LPW) Instrument for MAVEN. *Space Science Reviews*, *195*(1-4), 173–198. https://doi.org/10.1007/s11214-015-0194-3

André, M., & Yau, A. (1997). Theories and observations of ion energization and outflow in the high latitude magnetosphere. *Space Science Reviews*, *80*, 27–48. https://doi.org/10.1023/A:1004921619885

Ashour-Abdalla, M., & Kennel, C. (1978). Nonconvective and convective electron cyclotron harmonic instabilities. *Journal of Geophysical Research*, *83*(A4), 1531–1543. https://doi.org/10.1029/JA083iA04p01531

Benna, M., Mahaffy, P. R., Grebowsky, J. M., Fox, J. L., Yelle, R. V., & Jakosky, B. M. (2015). First measurements of composition and dynamics of the Martian ionosphere by MAVEN's Neutral Gas and Ion Mass Spectrometer. *Geophysical Research Letters*, *42*, 8958–8965. https://doi.org/10.1002/2015GL066146

Bertucci, C., Mazelle, C., Crider, D. H., Mitchell, D. L., Sauer, K., Acuña, M. H., & Winterhalter, D. (2004). MGS MAG/ER observations at the magnetic pileup boundary of Mars: Draping enhancement and low frequency waves. *Advances in Space Research*, *33*(11), 1938–1944. https://doi.org/10.1016/j.asr.2003.04.054

Brain, D. A., Bagenal, F., Acuña, M. H., Connerney, J. E. P., Crider, D. H., Mazelle, C., & Ness, N. F. (2002). Observations of low-frequency electromagnetic plasma waves upstream from the Martian shock. *Journal of Geophysical Research*, *107*(A6), 1076. https://doi.org/10.1029/2000JA000416

Brain, D. A., McFadden, J. P., Halekas, J. S., Connerney, J. E. P., Bougher, S. W., Curry, S., & Seki, K. (2015). The spatial distribution of planetary ion fluxes near Mars observed by MAVEN. *Geophysical Research Letters*, *42*, 9142–9148. https://doi.org/10.1002/2015GL065293

Collinson, G., Glocer, A., Xu, S., Mitchell, D., Frahm, R. A., Grebowsky, J., & Jakosky, B. (2019). Ionospheric ambipolar electric fields of Mars and Venus: Comparisons between theoretical predictions and direct observations of the electric potential drop. *Geophysical Research Letters*, *46*, 1168–1176. https://doi.org/10.1029/2018GL080597

Collinson, G., Wilson, L. B., Omidi, N., Sibeck, D., Espley, J., Fowler, C. M., & Jakosky, B. (2018). Solar wind induced waves in the skies of Mars: Ionospheric compression, energization, and escape resulting from the impact of ultralow frequency magnetosonic waves generated upstream of the Martian bow shock. *Journal of Geophysical Research: Space Physics*, *123*, 7241–7256. https://doi.org/10.1029/2018JA025414

Connerney, J. E. P., Espley, J. R., DiBraccio, G. A., Gruesbeck, J. R., Oliversen, R. J., Mitchell, D. L., & Jakosky, B. M. (2015). First results of the MAVEN magnetic field investigation. *Geophysical Research Letters*, *42*, 8819–8827. https://doi.org/10.1002/2015GL065366

Connerney, J. E. P., Espley, J., Lawton, P., Murphy, S., Odom, J., Oliversen, R., & Sheppard, D. (2015). The MAVEN magnetic field investigation. *Space Science Reviews*, *195*(1–4), 257–291. https://doi.org/10.1007/s11214-015-0169-4

Cui, J., Wu, X. S., Gu, H., Jiang, F. Y., & Wei, Y. (2019). Photochemical escape of atomic C and N on Mars: Clues from a multi-instrument MAVEN dataset. *Astronomy and Astrophysics*, *621*, A23. https://doi.org/10.1051/0004-6361/201833749

Dai, G., Su, Z., Liu, N., Wang, B., Zheng, H., Wang, Y., & Wang, S. (2019). Quenching of equatorial magnetosonic waves by substorm proton injections. *Geophysical Research Letters*, *46*, 6156–6167. https://doi.org/10.1029/2019GL082944

Ergun, R. E., Andersson, L., Peterson, W. K., Brain, D., Delory, G. T., Mitchell, D. L., & Yau, A. W. (2006). Role of plasma waves in Mars' atmospheric loss. *Geophysical Research Letters*, *33*, L14103. https://doi.org/10.1029/2006GL025785

Ergun, R. E., Morooka, M. W., Andersson, L. A., Fowler, C. M., Delory, G. T., Andrews, D. J., & Jakosky, B. M. (2015). Dayside electron temperature and density profiles at Mars: First results from the MAVEN Langmuir probe and waves instrument. *Geophyscial Research Letters*, *42*, 8846–8853. https://doi.org/10.1002/2015GL065280

Espley, J. R., Cloutier, P. A., Brain, D. A., Crider, D. H., & AcuñA, M. H. (2004). Observations of low-frequency magnetic oscillations in the Martian magnetosheath, magnetic pileup region, and tail. *Journal of Geophysical Research*, *109*, A07213. https://doi.org/10.1029/2003JA010193

Fowler, C. M., Agapitov, O. V., Xu, S., Mitchell, D. L., Andersson, L., Artemyev, A., & Mazelle, C. (2020). Localized heating of the Martian topside ionosphere through the combined effects of magnetic pumping by large-scale magnetosonic waves and pitch angle diffusion by whistler waves. *Geophysical Research Letters*, *47*, e2019GL086408. https://doi.org/10.1029/2019GL086408

Fowler, C. M., Andersson, L., Ergun, R. E., Harada, Y., Hara, T., Collinson, G., & Jakosky, B. M. (2018). MAVEN observations of solar wind-driven magnetosonic waves heating the Martian dayside ionosphere. *Journal of Geophysical Research: Space Physics*, *123*, 4129–4149. https://doi.org/10.1029/2018JA025208

Fowler, C. M., Andersson, L., Peterson, W. K., Halekas, J., Nagy, A. F., Ergun, R. E., & Jakosky, B. M. (2018). Correlations between enhanced electron temperatures and electric field wave power in the Martian ionosphere. *Geophysical Research Letters*, *45*, 493–501. https://doi.org/10.1002/2017GL073387

Fox, J. L. (1997). Upper limits to the outflow of ions at Mars: Implications for atmospheric evolution. *Geophysical Research Letters*, *24*(22), 2901–2904. https://doi.org/10.1029/97GL52842

Gombosi, T. I., & Nagy, A. F. (1989). Time-dependent modeling of field-aligned current-generated ion transients in the polar wind. *Journal of Geophysical Research*, *94*(A1), 359–369. https://doi.org/10.1029/JA094iA01p00359

Gurnett, D. A., Huff, R. L., Morgan, D. D., Persoon, A. M., Averkamp, T. F., Kirchner, D. L., & Picardi, G. (2008). An overview of radar soundings of the Martian ionosphere from the Mars Express spacecraft. *Advances in Space Research*, *41*(9), 1335–1346. https://doi.org/10.1016/j.asr.2007.01.062

Halekas, J. S., Brain, D. A., & Eastwood, J. P. (2011). Large-amplitude compressive "sawtooth" magnetic field oscillations in the Martian magnetosphere. *Journal of Geophysical Research*, *116*, A07222. https://doi.org/10.1029/2011JA016590

Hanson, W. B., Sanatani, S., & Zuccaro, D. R. (1977). The Martian ionosphere as observed by the Viking retarding potential analyzers. *Journal of Geophysical Research*, *82*(B28), 4351–4363. https://doi.org/10.1029/JS082i028p04351

Horne, R. B., Thorne, R. M., Glauert, S. A., Meredith, N. P., Pokhotelov, D., & Santolík, O. (2007). Electron acceleration in the Van Allen radiation belts by fast magnetosonic waves. *Geophysical Research Letters*, *34*, L17107. https://doi.org/10.1029/2007GL030267

Horne, R. B., Wheeler, G. V., & Alleyne, H. S. C. K. (2000). Proton and electron heating by radially propagating fast magnetosonic waves. *Journal of Geophysical Research*, *105*, 27,597–27,610. https://doi.org/10.1029/2000JA000018

Jakosky, B. M., Brain, D., Chaffin, M., Curry, S., Deighan, J., Grebowsky, J., & Zurek, R. (2018). Loss of the Martian atmosphere to space: Present-day loss rates determined from MAVEN observations and integrated loss through time. *Icarus*, *315*, 146–157. https://doi.org/10.1016/j.icarus.2018.05.030

Jakosky, B. M., Grebowsky, J. M., Luhmann, J. G., & Brain, D. A. (2015). Initial results from the MAVEN mission to Mars. *Geophysical Research Letters*, *42*, 8791–8802. https://doi.org/10.1002/2015GL065271

Jakosky, B. M., Lin, R. P., Grebowsky, J. M., Luhmann, J. G., Mitchell, D. F., Beutelschies, G., & Zurek, R. (2015). The Mars Atmosphere and Volatile Evolution ( MAVEN) mission. *Space Science Reviews*, *195*(1–4), 3–48. https://doi.org/10.1007/s11214-015-0139-x

Jeans, J. H. (1925). *The dynamical theory of gases* (4th ed.). New York: Cambridge University Press.

Johnson, R. E., Combi, M. R., Fox, J. L., Ip, W. H., Leblanc, F., McGrath, M. A., & Waite, J. H. (2008). Exospheres and atmospheric escape. *Space Science Reviews*, *139*(1–4), 355–397. https://doi.org/10.1007/s11214-008-9415-3

Liemohn, M. W., Khazanov, G. V., Moore, T. E., & Guiter, S. M. (1997). Self-consistent superthermal electron effects on plasmaspheric refilling. *Journal of Geophysical Research*, *102*(A4), 7523–7536. https://doi.org/10.1029/96JA03962

Luhmann, J. G., Johnson, R. E., & Zhang, M. H. G. (1992). Evolutionary impact of sputtering of the Martian atmosphere by $O^+$ pickup ions. *Geophysical Research Letters*, *19*(21), 2151–2154. https://doi.org/10.1029/92GL02485

Luhmann, J. G., Tatrallyay, M., Russell, C. T., & Winterhalter, D. (1983). Magnetic field fluctuations in the Venus magnetosheath. *Geophysical Research Letters*, *10*(8), 655–658. https://doi.org/10.1029/GL010i008p00655

Lundin, R., Barabash, S., Andersson, H., Holmström, M., Grigoriev, A., Yamauchi, M., & Bochsler, P. (2004). Solar wind-induced atmospheric erosion at Mars: First results from ASPERA-3 on Mars Express. *Science*, *305*(5692), 1933–1936. https://doi.org/10.1126/science.1101860

Lundin, R., Barabash, S., Dubinin, E., Winningham, D., & Yamauchi, M. (2011). Low-altitude acceleration of ionospheric ions at Mars. *Geophysical Research Letters*, *38*, L08108. https://doi.org/10.1029/2011GL047064

Matsumoto, H., & Nagai, K. (1981). Steepening, solution, and Landau damping of large-amplitude magnetosonic waves—Particle code computer simulation. *Journal of Geophysical Research*, *86*, 10,068–10,072. https://doi.org/10.1029/JA086iA12p10068

McElroy, M. B. (1972). Mars: An evolving atmosphere. *Science*, *175*(4020), 443–445. https://doi.org/10.1126/science.175.4020.443

McFadden, J. P., Kortmann, O., Curtis, D., Dalton, G., Johnson, G., Abiad, R., & Jakosky, B. (2015). MAVEN SupraThermal and Thermal Ion Composition (STATIC) instrument. *Space Science Reviews*, *195*(1–4), 199–256. https://doi.org/10.1007/s11214-015-0175-6

Moore, T. E., Chappell, C. R., Chandler, M. O., Craven, P. D., Giles, B. L., Pollock, C. J., & Mozer, F. S. (1997). High-altitude observations of the polar wind. *Science*, *277*(5324), 349–351. https://doi.org/10.1126/science.277.5324.349

Pepin, R. O. (1991). On the origin and early evolution of terrestrial planet atmospheres and meteoritic volatiles. *Icarus*, *92*(1), 2–79. https://doi.org/10.1016/0019-1035(91)90036-S

Porkolab, M. (1994). Plasma heating by fast magnetosonic waves in Tokamaks. *American Institute of Physics Conference Series*, *314*, 99–127. https://doi.org/10.1063/1.46754

Rönnmark, K. (1982). Waves in homogeneous, anisotropic, multicomponent plasmas. *Kiruna Geophysical Institute Bean Rep*, *179*, 55.

Shizgal, B. D., & Arkos, G. G. (1996). Nonthermal escape of the atmospheres of Venus, Earth, and Mars. *Reviews of Geophysics*, *34*(4), 483–505. https://doi.org/10.1029/96RG02213

Shklyar, D. R. (2017). Energy transfer from lower energy to higher-energy electrons mediated by whistler waves in the radiation belts. *Journal of Geophysical Research: Space Physics*, *122*, 640–655. https://doi.org/10.1002/2016JA023263

Sonnerup, B. U. O., & Cahill, J. (1967). Magnetopause structure and attitude from Explorer 12 observations. *Journal of Geophysical Research*, *72*, 171. https://doi.org/10.1029/JZ072i001p00171

Stix, T. H. (1992). *Waves in plasmas*. New York: American Institute of Physics.

Summers, D., Ni, B., & Meredith, N. P. (2007a). Timescales for radiation belt electron acceleration and loss due to resonant wave-particle interactions: 1. Theory. *Journal of Geophysical Research*, *112*, A04206. https://doi.org/10.1029/2006JA011801

Summers, D., Ni, B., & Meredith, N. P. (2007b). Timescales for radiation belt electron acceleration and loss due to resonant wave-particle interactions: 2. Evaluation for VLF chorus, ELF hiss, and electromagnetic ion cyclotron waves. *Journal of Geophysical Research*, *112*, A04207. https://doi.org/10.1029/2006JA011993

Varney, R. H., Solomon, S. C., & Nicolls, M. J. (2014). Heating of the sunlit polar cap ionosphere by reflected photoelectrons. *Journal of Geophysical Research: Space Physics*, *119*, 8660–8684. https://doi.org/10.1002/2013JA019378

Wei, Y., Fraenz, M., Dubinin, E., Woch, J., Lühr, H., Wan, W., & Dand ouras, I. (2012). Enhanced atmospheric oxygen outflow on Earth and Mars driven by a corotating interaction region. *Journal of Geophysical Research*, *117*, A03208. https://doi.org/10.1029/2011JA017340

Withers, P. (2009). A review of observed variability in the dayside ionosphere of Mars. *Advances in Space Research*, *44*(3), 277–307. https://doi.org/10.1016/j.asr.2009.04.027

Yau, A. W., & André, M. (1997). Sources of ion outflow in the high latitude ionosphere. *Space Science Reviews*, *80*, 1–25. https://doi.org/10.1023/A:1004947203046